IOP PUBLISHING JOURNAL OF PHYSICS D: APPLIED PHYSICS

J. Phys. D: Appl. Phys. **42** (2009) 175414 (9pp) doi:10.1088/0022-3727/42/17/175414

Optical and dielectric relaxor behaviour of $Ba(Zr_{0.25}Ti_{0.75})O_3$ ceramic explained by means of distorted clusters

T Badapanda[1], S K Rout[2], L S Cavalcante[3,6], J C Sczancoski[3], S Panigrahi[1], E Longo[4] and M Siu Li[5]

[1] Department of Physics, National Institute of Technology, Rourkela 769008, India
[2] Department of Applied Physics, Birla Institute of Technology, Mesra, Ranchi 835215, India
[3] Universidade Federal de São Carlos, PO Box 676, 13565-905, São Carlos, SP, Brazil
[4] Universidade Estadual Paulista, PO Box 355, 14801-907, Araraquara, SP, Brazil
[5] IFSC, Universidade de São Paulo, PO Box 369, 13560-970, São Carlos, SP, Brazil

E-mail: laeciosc@bol.com.br

Received 15 May 2009, in final form 26 July 2009
Published 20 August 2009
Online at stacks.iop.org/JPhysD/42/175414

Abstract

In this work, $Ba(Zr_{0.25}Ti_{0.75})O_3$ ceramic was prepared by solid-state reaction. This material was characterized by x-ray diffraction and Fourier transform Raman spectroscopy. The temperature dependent dielectric properties were investigated in the frequency range from 1 kHz to 1 MHz. The dielectric measurements indicated a diffuse phase transition. The broadening of the dielectric permittivity in the frequency range as well as its shifting at higher temperatures indicated a relaxor-like behaviour for this material. The diffusivity and the relaxation strength were estimated using the modified Curie–Weiss law. The optical properties were analysed by ultraviolet–visible (UV–vis) absorption spectroscopy and photoluminescence (PL) measurements at room temperature. The UV–vis spectrum indicated that the $Ba(Zr_{0.25}Ti_{0.75})O_3$ ceramic has an optical band gap of 2.98 eV. A blue PL emission was observed for this compound when excited with 350 nm wavelength. The polarity as well as the PL property of this material was attributed to the presence of polar $[TiO_6]$ distorted clusters into a globally cubic matrix.

(Some figures in this article are in colour only in the electronic version)

1. Introduction

In the last few years, the dielectric and optical properties of relaxor ferroelectrics have been widely investigated for applications in wireless communications, metal–oxide–semiconductor field-effect transistors, and optical and microwave dielectrics [1–6]. The main characteristics of relaxor ferroelectrics are the large, diffuse and frequency dispersive maximum in the temperature dependence of relative permittivity (ε) [7]. The relaxor behaviour has been studied in detail for lead-based perovskites, such as $PbTiO_3$ [8], $Pb(Zr,Ti)O_3$ [9] and $Pb(Mg,Nb)O_3$ [10]. However, these ceramics have serious drawbacks associated with the volatility and toxicity of PbO [11]. Therefore the chemical and physical properties of Pb-free compounds and their environmental friendliness have been investigated in order to improve the performance of electro-optic devices [12]. In particular, $BaTiO_3$-based ceramics are considered good candidates for this purpose due to their interesting properties, mainly including low dielectric constant, large tunability, low loss tangent and good thermal stability. Considering this class of ceramic materials, the good combination between the high dielectric constant and the low dissipation factor makes barium strontium titanate $(Ba,Sr)TiO_3$ (BST) a promising material for applications in dynamic random access memories (DRAMs) [13–15]. However, the high dielectric loss at high frequencies exhibited by this ceramic limits its use as a microwave dielectric [16, 17].

Currently, barium zirconate titanate $Ba(Zr_xTi_{1-x})O_3$ (BZT) has been chosen as an alternative material to replace

[6] Author to whom any correspondence should be addressed.

 © 2009 IOP Publishing Ltd Printed in the UK

BST in the fabrication of ceramic capacitors, since $[ZrO_6]$ clusters are chemically more stable than those of $[TiO_6]$ [18–22]. Generally, this material is formed by a solid solution between barium titanate ($BaTiO_3$) and barium zirconate ($BaZrO_3$), where its dielectric properties and phase transition temperature (T_m) (from ferroelectric to paraelectric) are strongly dependent on Zr content into the lattice. For compositions with zirconium (Zr) content up to $x = 0.05$, BZT presents a perovskite-type rhombohedral structure at room temperature [23]. When the Zr content is increased up to $x \geqslant 0.08$, BZT crystallizes in an orthorhombic structure and exhibits a broad permittivity–temperature ($\varepsilon \sim T$) curve near T_m, which is caused by the inhomogeneous distribution of $[ZrO_6]$ clusters into the titanium (Ti) sites and/or by the mechanical stresses on the grains [24]. A structural transition from tetragonal to pseudocubic is verified in BZT compounds when the Zr content is increased up to $x \approx 0.20$ into the matrix [25]. In fact, this composition is responsible for the phase transition from ferroelectric to relaxor in these materials. Ravez and Simon [26] reported a typical relaxor-like behaviour in BZT ceramics with Zr content up to $x \geqslant 0.25$. Tang *et al* [27] observed a 'slim' hysteresis loop in BZT ceramics with high Zr contents ($x = 0.30$ and 0.35). According to these authors, this typical relaxor behaviour is ascribed to the existence of micropolar regions into the lattice.

Recently, studies on the optical properties of crystalline and non-crystalline BZT thin films or bulk ceramics have been mainly focused on the infrared optical properties [28, 29], complex refractive index [30–32] and photoluminescence (PL) [33–36]. In particular, the PL properties have been observed only in BZT thin films and powders prepared by the polymeric precursor method.

Therefore, we report on the microstructure, relaxor dielectric and optical properties of $Ba(Zr_{0.25}Ti_{0.75})O_3$ ceramics prepared by solid-state reaction (SSR). This material was structurally characterized by x-ray diffraction (XRD) and Fourier transform Raman (FT-Raman) spectroscopy. The relaxor dielectric properties were investigated by means of the dielectric constant and dielectric loss measurements as a function of temperature. The optical properties were analysed by ultraviolet–visible (UV–vis) absorption spectroscopy and PL measurements at room temperature.

2. Experimental procedure

2.1. Synthesis and characterization of $Ba(Zr_{0.25}Ti_{0.75})O_3$ ceramic by SSR

$Ba(Zr_{0.25}Ti_{0.75})O_3$ ceramic was prepared by SSR. In this synthesis method, barium carbonate ($BaCO_3$) (99.0%, S D Fine Chemicals, Mumbai), titanium oxide (TiO_2) (99.0%, E Merck, India Ltd) and zirconium oxide (ZrO_2) (99.0%, Loba Chemicals, Mumbai) were used as raw materials. These compounds were stoichiometric mixed using isopropyl alcohol (IPA) and milled using an agate mortar to obtain a homogeneous powder. Afterwards, this powder was heat treated successively at 1573 K for 4 h with repeated cycles of mixing and grinding. Finally, the pure $Ba(Zr_{0.25}Ti_{0.75})O_3$ phase was obtained when the sintering process was performed at 1673 K for 6 h.

$Ba(Zr_{0.25}Ti_{0.75})O_3$ ceramic was structurally characterized by XRD using a DMax/2500PC diffractometer (Rigaku, Japan). XRD patterns were obtained using Cu Kα radiation in the 2θ range from 10° to 75° with a scanning rate of 0.02° min^{-1}. FT-Raman measurements were performed using a Bruker-RFS/100. The spectrum was obtained with a Nd : YAG ion laser ($\lambda = 1064$ nm), keeping its maximum output power at 45 mW. The average grain size was estimated with a JSM T330 scanning electron microscope (Jeol, USA) operated at 25 keV. In order to measure the electrical properties of $Ba(Zr_{0.25}Ti_{0.75})O_3$ ceramic, discs were pressed uniaxially at 200 MPa with 2 wt% polyvinyl alcohol added as a binder. Afterwards, these discs were sintered at 1623 K for 4 h. The disc densities were estimated at approximately 5.96 g cm^{-3} by the Archimedes' principle. Silver contacts were deposited on the opposite disc faces and heated at 973 K for 5 min. The dielectric measurements were carried out in the frequency range from 1 KHz to 1 MHz using an impedance analyzer (HP 4192A, USA) connected to a computer. The dielectric data were collected at an interval of 3 K, keeping a heating rate of 0.5 K min^{-1}. The UV–vis spectrum was taken using a Cary 5G (Varian, USA) spectrophotometer in diffuse reflection mode. PL measurements were performed through a Monospec 27 monochromator (Thermal Jarrel Ash, USA) coupled to a R446 photomultiplier (Hamamatsu, Japan). A krypton ion laser (Coherent Innova 90K, USA) ($\lambda = 350$ nm) was used as an excitation source, keeping its maximum output power at 200 mW. The UV–vis and PL spectra were taken three times for each sample in order to ensure the reliability of the results. All measurements were performed at room temperature.

3. Results and discussion

3.1. XRD analysis and clusters models

Figure 1 shows the XRD patterns of $Ba(Zr_{0.25}Ti_{0.75})O_3$ ceramic sintered at 1673 K for 6 h.

In this figure, all diffraction peaks were indexed to the perovskite-type cubic structure with space group $Pm\bar{3}m$, in agreement with the respective Joint Committee on Powder Diffraction Standards (JCPDS) card no 36-0019 [37]. Moreover, the sharp and well-defined diffraction peaks indicate that this ceramic material has a degree of crystallinity at long range. The lattice parameters and unit cell volume were estimated through the UNITCELL-97 program [38] using the regression diagnostics combined with nonlinear least squares. The obtained unit cell data for the $Ba(Zr_{0.25}Ti_{0.75})O_3$ ceramic were $a = b = c = 4.05$ Å and $V = 66.43$ $Å^3$, confirming the cubic structure.

Figure 2 shows a schematic representation of ordered $Ba(Zr_{0.25}Ti_{0.75})O_3$ supercell ($1 \times 2 \times 2$).

In this supercell, the Zr and Ti atoms are bonded to six oxygens ($[ZrO_6]$ and $[TiO_6]$ clusters), forming a polyhedron-type with octahedral configuration (figure 2). In principle, this crystalline structure is characterized by a high

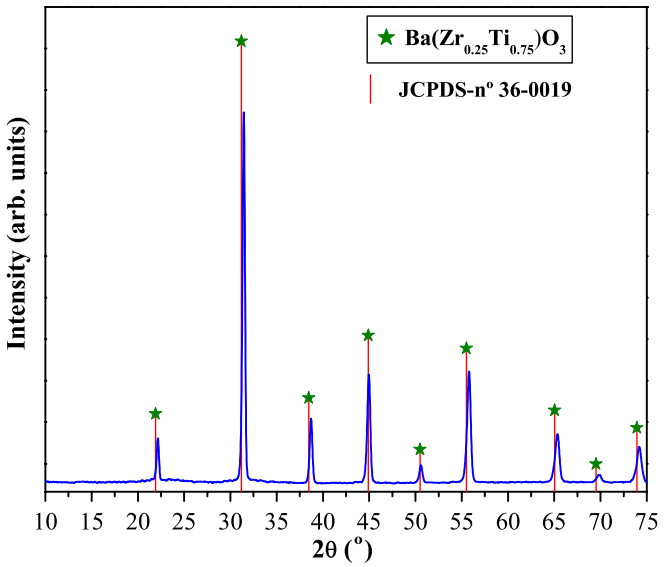

Figure 1. The XRD pattern of $Ba(Zr_{0.25}Ti_{0.75})O_3$ ceramic.

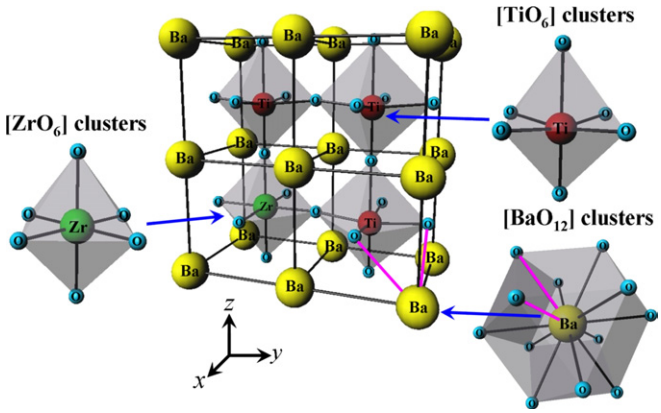

Figure 2. Schematic representation of a cubic $Ba(Zr_{0.25}Ti_{0.75})O_3$ supercell, illustrating the $[TiO_6]$, $[ZrO_6]$ and $[BaO_{12}]$ clusters.

degree of symmetry on the non-polar $[ZrO_6]$ clusters and distortions on the polar $[TiO_6]$ clusters. These distortions arise from a difference in the covalent character between the O–Ti–O and O–Zr–O bonds (directional orientations) into the structure [39, 40]. On the other hand, the Ba atoms are coordinated to twelve oxygens ($[BaO_{12}]$ clusters), resulting in a dodecahedron-type geometry. The existence of polar $[TiO_6]$ clusters close to $[BaO_{12}]$ clusters (ionic bond with radial orientation) causes the structural order–disorder into the cubic $Ba(Zr_{0.25}Ti_{0.75})O_3$ matrix, contributing to the polarization processes into the system. References [41, 42] report that the coordination as well as the local non-centrosymmetry into the lattice of a particular material can be identified by means of x-ray absorption near-edge structure and extended x-ray absorption fine structure techniques.

3.2. FT-Raman analysis

Figure 3 shows the FT-Raman spectrum of $Ba(Zr_{0.25}Ti_{0.75})O_3$ ceramic prepared by SSR and sintered at 1673 K for 6 h.

The Raman-active modes indicate the presence of structural distortions at short range in this material. In this

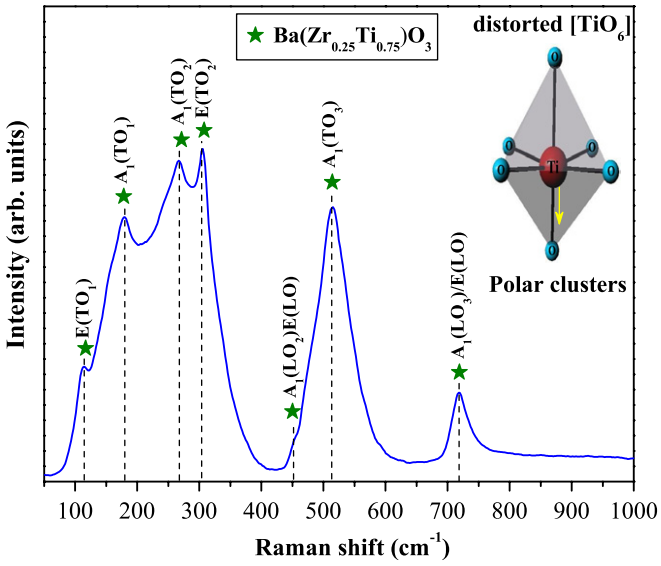

Figure 3. FT-Raman spectrum of $Ba(Zr_{0.25}Ti_{0.75})O_3$ ceramic.

case, it was possible to identify seven Raman-active modes in the FT-Raman spectrum of $Ba(Zr_{0.25}Ti_{0.75})O_3$ ceramic, where two are overlapping. These modes are classified into longitudinal (LO) and transverse (TO) components because of the long-range electrostatic forces associated with the lattice ionicity [43, 44]. In this Raman spectrum, the $A_1(TO_1)$ and $A_1(TO_3)$ modes situated at around 180 and 514 cm^{-1} are ascribed to the (O–Ti–O–Zr–O) stretching symmetric or asymmetric vibrations [45, 46]. The $E(TO_1)$ and $E(TO_2)$ modes detected at around 114 and 305 cm^{-1} are related to the phase transition from tetragonal to cubic [47]. These modes do not indicate that the $Ba(Zr_xTi_{1-x})O_3$ with Zr content $x = 0.25$ has a tetragonal structure, but they suggest that in this cubic structure there are polar $[TiO_6]$ distorted clusters. In particular, the $E(TO_2)$ stretching mode is arising from the formation of $[TiO_6]$ clusters at short range. The low intensity of this mode when compared with the $BaTiO_3$ [48] can be due to the non-polar $[ZrO_6]$ clusters, which are able to reduce the dipolar interactions between the polar $[TiO_6]$ clusters [49] (inset). The $A_1(LO_3)$ mode verified at 718 cm^{-1} is because of the sites containing polar $[TiO_6]$ clusters or hexa-coordinated Ti species [49]. The other modes arise from lattice vibrations in the LO and TO directions.

3.3. Scanning electron microscope analysis

Figure 4 shows a typical SEM micrograph of $Ba(Zr_{0.25}Ti_{0.75})O_3$ ceramic prepared by SSR and sintered at 1673 K for 6 h.

As can be seen in this micrograph, the $Ba(Zr_{0.25}Ti_{0.75})O_3$ ceramic is composed of large grains with an average size of approximately 10 μm. We believe that these morphological characteristics are governed by the matter transport mechanism between the grains during the sintering process. In principle, in the initial stages of SSR, the carbonates and oxides ($BaCO_3$, TiO_2 and ZrO_2) used to form the $Ba(Zr_{0.25}Ti_{0.75})O_3$ phase are well mixed and constantly milled in order to reduce the powder particle sizes. The heat treatment performed at 1573 K for 4 h promotes a slow kinetics of interdiffusion in the contact

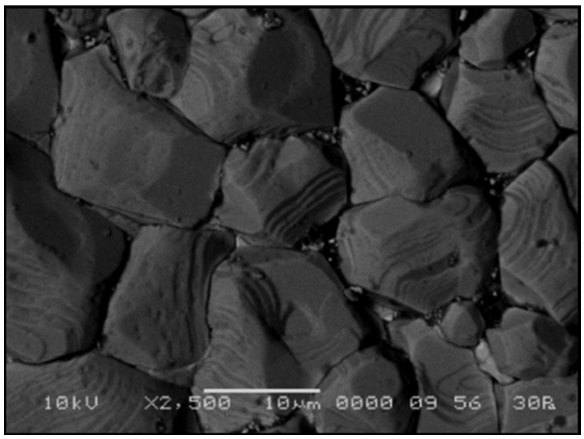

Figure 4. SEM micrograph of $Ba(Zr_{0.25}Ti_{0.75})O_3$ ceramic.

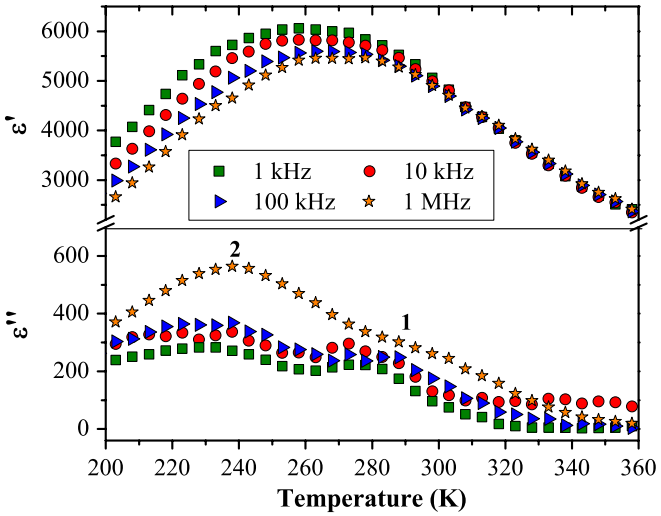

Figure 5. Temperature dependence of real and imaginary permittivity at different frequencies for the $Ba(Zr_{0.25}Ti_{0.75})O_3$ ceramic.

points between the particles with irregular morphologies [50]. Probably, this diffusion process leads to the formation of necks between the grains due to an elastic deformation caused by the surface energy reduction in the contact interface [51]. The neck growth is favoured by the long sintering time, allowing the matter transport at long distances [52]. In this process, the grain boundaries play a fundamental role in the material transport into the system. The formation of large grains with irregular shapes could be a result of the variations on the kinetics of movement from boundary to boundary, since the grain-boundary energy is dependent on the grain-boundary orientation and grain-boundary mobility [52]. When the sintering process was performed at 1673 K for 6 h, the grain growth process was intensified, causing a reduction in the number of pores and disappearing with some grains, generally the smaller ones [51]. In figure 4, the occurrence of grooves between the grains was also observed. According to [53], this phenomenon is caused by a capillarity driven process, where the grain boundary emerges to intersect a free surface [54]. In this case, the system seeks to minimize the combined energy of the grain boundary and the free surface by developing a groove at the point of intersection. The excess energy associated with the grain boundary provides the driving force to sustain the grooving process.

3.4. Dielectric spectroscopy analysis

Figure 5 shows the temperature dependence of relative real and imaginary dielectric permittivity performed at different frequencies (1 kHz, 10 kHz, 100 kHz and 1 MHz) for the $Ba(Zr_{0.25}Ti_{0.75})O_3$ ceramic prepared by SSR and sintered at 1673 K for 6 h.

The real permittivity (ε') value gradually increases up to a maximum value (ε_m) with the increase of temperature, and then it smoothly decreases, suggesting a phase transition. The maximum relative permittivity (ε_m) as well as its corresponding temperature (T_m) is dependent on the frequency. In this case, the relative dielectric permittivity magnitude decreases with the increase in the frequency, shifting the maximum value (ε_m) to higher temperatures. Hence, this result indicates that the dielectric polarization has a relaxation-type behaviour. As can be seen in figure 5, the dielectric loss value corresponding to the ferroelectric phase was substantially reduced at room temperature up to the paraelectric phase (above T_m). Probably, the frequency dispersion at lower temperatures (below T_m) is because of the presence of space charges.

The high dielectric loss value at 1 kHz can be related to the different types of polarization and/or caused by the finite resistivity of the material. Moreover, the increase of the ε'' values in the region of low temperatures could be arising from the increase in the ionic conductivity as a consequence of a local disorder or displacement between the Ti–O, Zr–O, Ba–O bonds. In this case, this symmetric break induces the charge mobility into the octahedral clusters [55]. In figure 5, when the frequency was increased, an increase in the dielectric loss with the temperature evolution was verified. This result indicates that the dielectric polarization is caused by a relaxation type as those observed in dipolar glasses [56]. Also, two relaxation peaks were observed in the graph corresponding to the ε'' as a function of temperature. The first, one located at 240 K, is generally ascribed to the transition from crystalline to glassy phase, while the second one, at 290 K, represents the molecular motion of the glass phase. In analogy with spin glasses, the dynamic susceptibility behaviour in disordered ferroelectrics is supposed to be associated with a broad spectrum of relaxation times. Generally, it is considered that the Debye model is based on the assumption of a single relaxation time. Thus, this model fails when employed for a relaxation time distribution. On the assumption of a relaxation time distribution, this implies that the local environment seen by individual dipoles differs from site to site. As a rule [57], this relaxation process occurs in disordered ionic structures, particularly in solid solution. In the Curie temperature range, the relative dielectric permittivity exhibits high values with large dispersions, which is found in orientated glasses [56]. Qualitatively, the strong and broad dielectric peak indicates that the phase transition is diffuse type near the transition temperature (T_m). This phenomenon can be related to the inhomogeneous distribution of $[ZrO_6]$ clusters into the Ti sites and/or by the mechanical stresses on

the grains [58]. At 10 kHz, the maximum relative dielectric permittivity (ε_m) of $Ba(Zr_{0.25}Ti_{0.75})O_3$ ceramic was detected at 267 K (T_m).

This decrease in the Curie temperature can be explained on the basis of modified Landau–Ginzburg–Devonshire (LGD) phenomenological theory [59], which is described by the following equation: $T_c/T_{c_0} = (1-K)/D$, where K is the material constant ($K = 2S_oD_o/3R$), T_c is the size dependent Curie temperature, D is the crystal diameter, S_0 is the transition entropy, D_0 is the critical particle size where the ferroelectric phase does not exist and R is the ideal gas constant. The effect of grain size on the transition temperature is associated with the high surface tensions on the small grains, which act the same way as the hydrostatic pressure, reducing the Curie point. In addition, the forces experienced by the ions near or far from the grain surface are not equivalent. Therefore, these considerations suggest that there is a quadratic gradient between the grain bulk and surface. However, for small grain sizes, the superficial grain layers represent a significant fraction, which are able to influence the structural and dielectric properties. The diffuse transition nature, especially in the case of ferroelectric ceramics, is usually attributed to the grain size distribution and/or a quadratic gradient, leading to a transition temperature distribution. This phenomenon is more pronounced in samples containing both $[TiO_6]$ and $[ZrO_6]$ clusters in its compositions, probably as a consequence of the difference in the electronic density between the polar $[TiO_6]$ and non-polar $[ZrO_6]$ clusters. Hence, the additional spatial fluctuations caused by the $[TiO_6]$ and $[ZrO_6]$ clusters into the structure lead to the coexistence of regions with different Curie temperatures, which are dependent on the Ti and Zr concentrations in the solid solution [60]. A diffuse phase transition is commonly observed by the broadening of the dielectric constant (ε) as a function of temperature (T). The large separation (in temperature) between the maximum real and imaginary (dielectric loss) points from the dielectric constant curve, deviation from the Curie–Weiss law near T_m, frequency dispersion of both dielectric and dielectric loss in the transition region imply a frequency dependence with T_m [61–63].

Figure 6 shows the inverse dielectric constant as a function of temperature performed at different frequencies (1 kHz, 10 kHz, 100 kHz and 1 MHz) for the $Ba(Zr_{0.25}Ti_{0.75})O_3$ ceramic prepared by SSR sintered at 1673 K for 6 h.

A deviation from the Curie–Weiss law can be observed for all frequencies (figure 6). This deviation is a typical behaviour of ferroelectric materials with diffuse phase transition. The parameter ΔT_m describes the degree of deviation from the Curie–Weiss law and is defined as $\Delta T_m = T_{cw} - T_m$, where T_{cw} denotes the temperature where the dielectric permittivity starts to deviate from the Curie–Weiss law and T_m is the temperature of the dielectric maximum [64]. The Curie temperature is determined from the graph by the extrapolation of the reciprocal dielectric constant in the paraelectric region. The obtained results are displayed in table 1.

A modified Curie–Weiss law has been proposed to describe the diffuseness in a phase transition [65, 66]:

$$\frac{1}{\varepsilon'} - \frac{1}{\varepsilon_m} = \frac{(T-T_m)^\gamma}{C'}, \qquad (1)$$

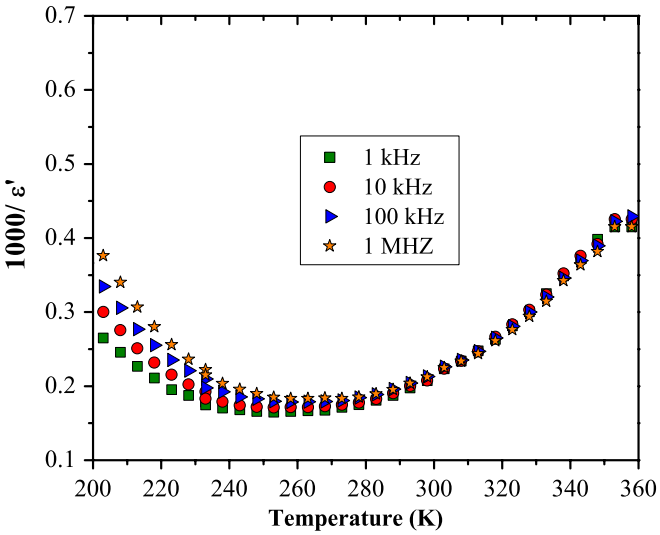

Figure 6. Inverse dielectric constant as a function of temperature at different frequencies for the $Ba(Zr_{0.25}Ti_{0.75})O_3$ ceramic.

Table 1. Parameters obtained through the dielectric data as a function of temperature at different frequencies for the $Ba(Zr_{0.25}Ti_{0.75})O_3$ ceramic.

Frequency	T_m (K)	T_0 (K)	ΔT_m (K)	ε_m	T_{cw} (K)
1 kHz	258	296	75	6062	333
10 kHz	263	303	80	5836	343
100 kHz	274	308	88	5572	361
1 MHz	284	321	90	5420	374

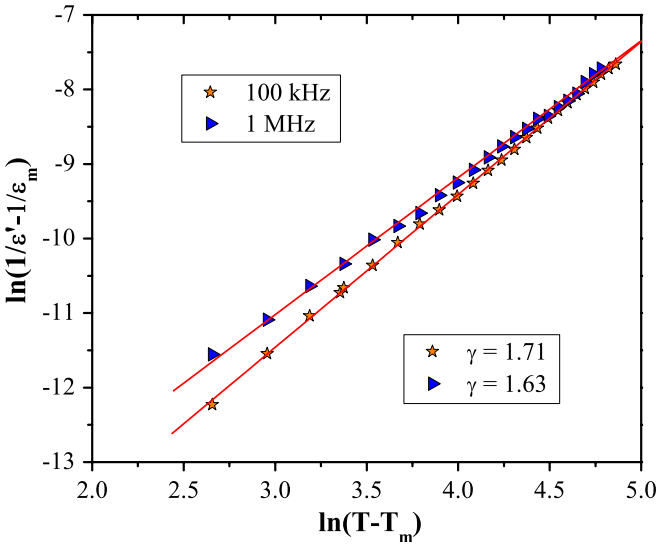

Figure 7. $\ln(1/\varepsilon' - 1/\varepsilon_m)$ as a function of $\ln(T - T_m)$ at frequencies of 100 kHz and 1 MHz.

where both γ and C' are constants. The parameter γ gives information on the phase transition character ($\gamma = 1 \rightarrow$ a normal Curie–Weiss law is obtained and $\gamma = 2 \rightarrow$ it reduces to the quadratic dependence which describes a complete diffuse phase transition).

Figure 7 shows the graph of $\ln(1/\varepsilon' - 1/\varepsilon_m)$ as a function of $\ln(T - T_m)$ at frequencies of 100 kHz and 1 MHz, respectively.

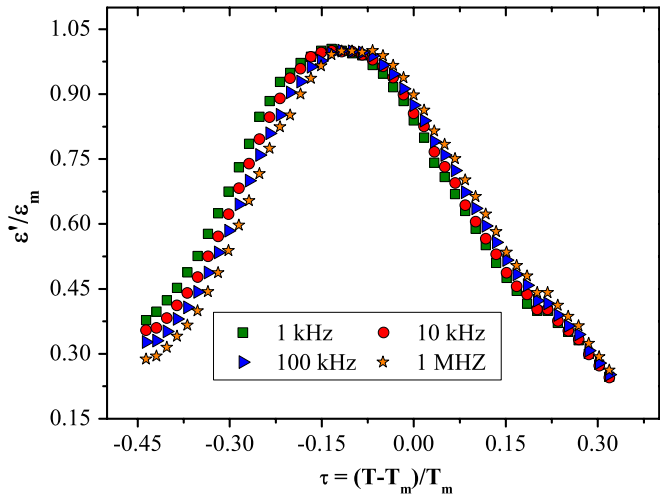

Figure 8. Reduced dielectric constant ($\varepsilon'/\varepsilon_m$) as a function of reduced temperature [$\tau = (T - T_m)/T_m$] at different frequencies for the $Ba(Zr_{0.25}Ti_{0.75})O_3$ ceramic.

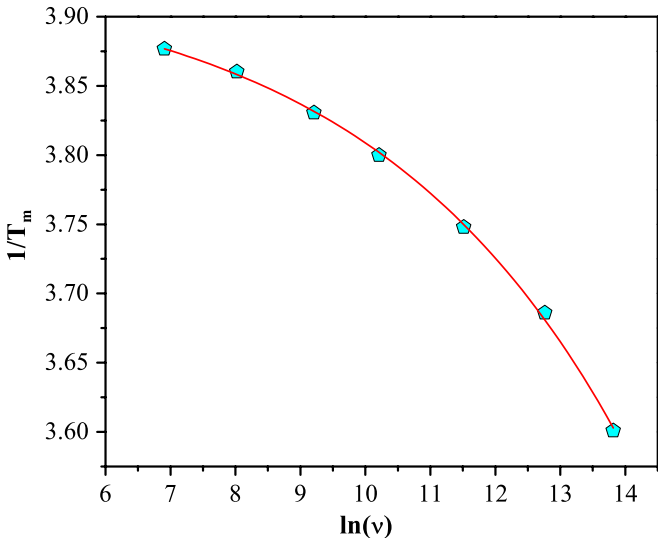

Figure 9. $1/T_m$ as function of $\ln(\nu)$ for the $Ba(Zr_{0.25}Ti_{0.75})O_3$ ceramic. The spheres are the experimental points and the line is the Vogel–Fulcher relation.

The γ value was found to be 1.71 for 100 kHz and 1.63 for 1 MHz, respectively. An important observation on the fit performed in our experimental data by means of equation (1) indicated that a universal γ value was not obtained in the temperature range above T_m. The γ value continuously approaches unity when it departs from T_m. This value suggests that the material has structural order–disorder and diffuse phase transition. The observed broadness or diffusiveness occurs mainly because of the compositional fluctuation and/or due to the structural disorder into the lattice by the [TiO_6] and [BaO_{12}] clusters (figure 2). This behaviour suggests a microscopic heterogeneity into the $Ba(Zr_{0.25}Ti_{0.75})O_3$ structure, presenting different local Curie points. The nature and variation of the dielectric constant as well as the presence of non-polar [ZrO_6] clusters indicate that the material has a ferroelectric–relaxor phase transition.

The broadening in the phase transition is better illustrated in figure 8, which shows the graph of the reduced dielectric constant ($\varepsilon'/\varepsilon_m$) as a function of reduced temperature [$\tau = (T - T_m)/T_m$] at different frequencies (1 kHz, 10 kHz, 100 kHz and 1 MHz).

The slight deviations noted in the full width of the curves at different frequencies are analogous to those observed in other relaxor materials [67, 68]. For a more detailed insight into the relaxation process in the relative dielectric permittivity, a graph of $1/T_m$ was plotted as a function of $\ln(\nu)$, as shown in figure 9.

In this figure, the nonlinear nature indicates that the data cannot be fitted by the simple Debye equation. In order to analyse the relaxation characteristics of $Ba(Zr_{0.25}Ti_{0.75})O_3$ ceramic, the experimental curves were fitted using the Vogel–Fulcher equation [69, 70]:

$$\nu = \nu_0 \exp\left[\frac{-E_a}{k_B(T_m - T_f)}\right], \tag{2}$$

where ν_0 is the attempt frequency, E_a is the measure of average activation energy, k_B is the Boltzman constant and T_f is the freezing temperature. The T_f is considered as the temperature where the dynamic reorientation of distorted [TiO_6] clusters leads to polarization in the lattice. The fitting parameters were $T_f = 128$ K, $E_a = 0.15$ eV and $\nu_0 = 1.03 \times 10^{11}$ Hz. The empirical relaxation strength described by the frequency dispersion of T_m is defined as

$$\Delta T_{res} = T_{m(1\,MHz)} - T_{m(10\,kHz)}, \tag{3}$$

where ΔT_{res} is derived from the dielectric measurement of the ceramic compound. In our work, this value is approximately 17.14 K.

3.5. UV–vis absorption spectroscopy analysis

Figure 10 shows the UV–vis absorbance spectrum of $Ba(Zr_{0.25}Ti_{0.75})O_3$ ceramic prepared by SSR and sintered at 1673 K for 6 h. The inset illustrates a proposed model where the intermediary energy levels within the band gap of $Ba(Zr_{0.25}Ti_{0.75})O_3$ are basically composed of oxygen 2p states situated near the valence band as well as titanium 3d and zirconium 4d states located below the conduction band (deep and shallow holes).

The optical band gap energy (E_{gap}) was estimated by the method proposed by Wood and Tauc [71]. According to these authors the optical band gap is associated with the absorbance and photon energy by the following equation:

$$h\nu\alpha \propto (h\nu - E_{gap})^n, \tag{4}$$

where α is the absorbance, h is the Planck constant, ν is the frequency, E_{gap} is the optical band gap and n is a constant associated with the different types of electronic transitions ($n = 1/2, 2, 3/2$ or 3 for direct allowed, indirect allowed, direct forbidden and indirect forbidden transitions, respectively). Thus, the E_{gap} value of $Ba(Zr_{0.25}Ti_{0.75})O_3$ ceramic was evaluated extrapolating the linear portion of the curve or tail. In our work, the UV–vis absorbance spectrum

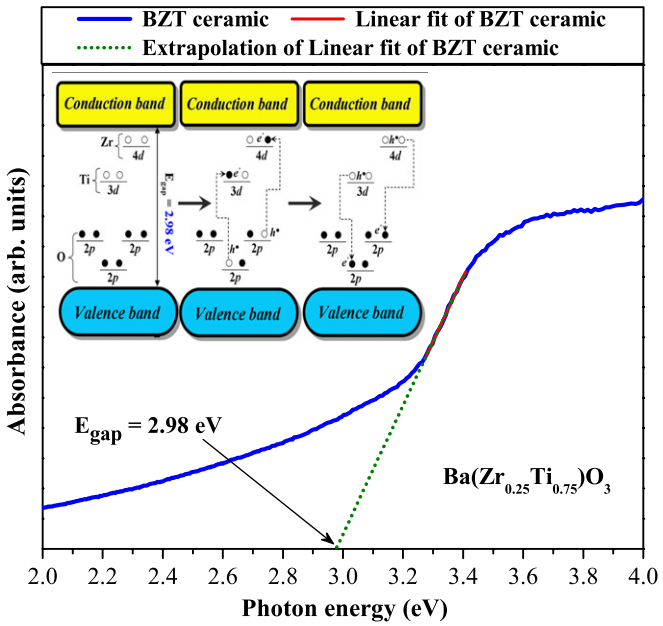

Figure 10. The UV–vis absorbance spectrum of $Ba(Zr_{0.25}Ti_{0.75})O_3$ ceramic. Inset illustrates a wide band model composed of deep and shallow holes within the band gap.

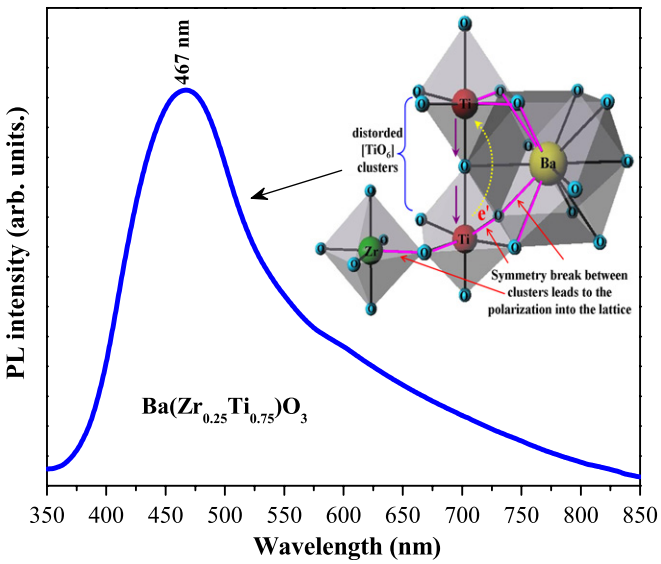

Figure 11. PL spectrum at room temperature of $Ba(Zr_{0.25}Ti_{0.75})O_3$ ceramic. Inset shows a possible charge transfer process between the clusters.

suggests an indirect allowed transition and, therefore, the $n = 2$ was used in equation (4).

In principle, we believe that the obtained E_{gap} value for the $Ba(Zr_{0.25}Ti_{0.75})O_3$ ceramic can be associated with an effect of structural order–disorder into the lattice due to a symmetry break between the O–Ti–O bonds and/or distortions on the $[TiO_6]$ clusters. A plausible explication for the origin of this symmetry break can be related to the synthesis method. It is possible to conclude on this hypothesis that the high temperatures employed in the SSR during the sintering process are not sufficient to avoid the structural defects (symmetry break between bonds or distortions) into the $Ba(Zr_{0.25}Ti_{0.75})O_3$ structure, mainly those arising from the repeated cycles of grinding. Consequently, these structural defects induce the formation of intermediary energy levels within the band gap, which are basically composed of oxygen 2p states situated near the valence band as well as titanium 3d and zirconium 4d states located below the conduction band (deep and shallow holes) [72]. Reference [73] reports that the deep holes are responsible for the green, yellow, orange and red PL emission at room temperature, while the shallow holes promote the violet and blue emissions.

3.6. PL analysis

Figure 11 shows the PL spectrum of $Ba(Zr_{0.25}Ti_{0.75})O_3$ ceramic prepared by SSR and sintered at 1673 K for 6 h. The inset illustrates a possible break symmetry caused by the distorted $[TiO_6]$ clusters into the lattice.

This broad PL profile suggests an emission mechanism characterized by the contribution of several energy levels (or light emission centres) during the excitation and emission processes of photons. When excited with 350 nm wavelength, this compound exhibited a low PL emission with the maximum situated at around 467 nm (blue emission), suggesting that there is a greater contribution of the shallow holes than the deep holes within the band gap. We believe in this hypothesis, since the excitation energy (350 nm $\approx$ 3.54 eV) is higher than the E_{gap} value exhibited for this crystalline material. As previously described in the text, the origin of these intermediary energy levels is due to the symmetry break between the O–Ti–O bonds and/or distortions on the $[TiO_6]$ clusters, which are induced by the SSR method.

4. Conclusions

In summary, the $Ba(Zr_{0.25}Ti_{0.75})O_3$ ceramic was prepared by the SSR method. XRD patterns showed that this material crystallizes in a perovskite-type cubic structure with space group $Pm\bar{3}m$. The existence of Raman-active modes was associated with the structural distortions caused by the polar $[TiO_6]$ distorted clusters at short range into the lattice. The SEM micrographs indicated that this material is composed of large grains ($\approx$10 μm) with irregular shapes. These microstructural characteristics were attributed to the matter transport mechanisms via grain boundary during the sintering process. The distortion on the $[TiO_6]$ clusters leads to a charge redistribution and polarization in the lattice. The relaxation-type behaviour was observed through the reduction in the relative dielectric permittivity with an increase in the frequency as well as by the broad dielectric peak near the transition temperature (T_m). The critical exponent value ($\gamma = 1.71$ at 100 kHz and $\gamma = 1.63$ at 1 MHz) obtained from the modified Curie–Weiss law suggests a strong relaxation behaviour. The experimental T_m data indicated good agreement with the Vogel–Fulcher equation. The empirical parameters (ΔT_m, ΔT_{res} and ΔT_{cw}) confirmed the relaxor behaviour for the $Ba(Zr_{0.25}Ti_{0.75})O_3$ ceramic. Finally, the origin of the blue PL emission was related to the intermediary energy levels within the band gap, where the greater contribution was attributed to the shallow holes situated near the conduction band.

Acknowledgments

The authors acknowledge the financial support of the Brazilian research financing institutions: CAPES, CNPq and FAPESP. Special thanks to Professor Dr Sanjeeb Kumar Rout for consolidating the partnership of this research between India and Brazil.

References

[1] Cross L E 1987 *Ferroelectrics* **76** 241
[2] Bokov A A and Ye Z G 2006 *J. Mater. Sci.* **41** 31
[3] Sebastian M T 2008 *Dielectric Materials for Wireless Communication* (Amsterdam: Elsevier) p 58, chapter 3
[4] Dimitrakopoulos C D, Kymissis I, Purushothaman S, Neumayer D A, Duncombe P R and Laibowitz R B 1999 *Adv. Mater.* **11** 1372
[5] Xu J, Menesklou W and Ivers-Tiffée E 2005 *J. Eur. Ceram. Soc.* **25** 2289
[6] Xu J B, Zhai J W and Yao X 2007 *Ferroelectrics* **357** 730
[7] Bokov A A, Maglione M and Ye Z G 1999 *J. Phys.: Condens. Matter* **19** 092001
[8] Zeng H, Lu S, Dai L, Liu J, Wang Z and Zuo C 2005 *Mater. Lett.* **59** 2808
[9] Okayasu M, Aoki S and Mizuno M 2008 *Int. J. Fatigue* **30** 1115
[10] Chaipanich A and Tunkasiri T 2007 *Curr. Appl. Phys.* **7** 281
[11] Maiti T, Guo R and Bhalla A S 2008 *J. Am. Ceram. Soc.* **91** 1769
[12] Wang X and Yang A 2009 *J. Phys. D: Appl. Phys.* **42** 075419
[13] Kotecki D E *et al* 1999 *IBM J. Res. Dev.* **43** 367
[14] Yoon D S, Roh J S, Baik H K and Lee S M 2002 *Crit. Rev. Solid State Mater. Sci.* **27** 143
[15] Yoshida M *et al* 1996 *NEC Res. Dev.* **37** 305
[16] Tagantsev A K, Sherman V O, Astafiev K F, Venkatesh J and Setter N 2003 *J. Electroceram.* **11** 55
[17] Zimmermann F, Voigts M, Menesklou W and Ivers-Tiffée E 2004 *J. Eur. Ceram. Soc.* **24** 1729
[18] Zhi Y, Chen A, Guo R and Bhalla A S 2002 *Appl. Phys. Lett.* **81** 1285
[19] Tsurumi T, Yamamoto Y, Kakemoto H and Wada S 2002 *J. Mater. Res.* **17** 755
[20] Ravez J, Broustera C and Simon A 1999 *J. Mater. Chem.* **9** 1609
[21] Yu Z, Guo R and Bhalla A S 2000 *Appl. Phys. Lett.* **77** 1535
[22] Qin W F, Xiong J, Zhu J, Tang J L, Jie W J, Zhang Y and Li Y R 2008 *J. Mater. Sci.* **43** 409
[23] Moura F, Simões A Z, Stojanovic B D, Zaghete M A, Longo E and Varela J A 2008 *J. Alloys Compounds* **462** 129
[24] Weber U, Greuel G, Boettger U, Weber S, Hennings D and Waser R 2001 *J. Am. Ceram. Soc.* **84** 759
[25] Hennings D, Schnell A and Simon G 1982 *J. Am. Ceram. Soc.* **65** 539
[26] Ravez J and Simon A 1997 *Eur. J. Solid State Inorg. Chem.* **34** 1199
[27] Tang X G, Chew K H and Chan H L W 2004 *Acta Mater.* **52** 5177
[28] Xu J, Gao C, Zhai J, Yao X, Xue J and Huang Z 2006 *J. Cryst. Growth* **291** 130
[29] Liu A, Xue J, Meng X, Sun J, Huang Z and Chu J 2008 *Appl. Surf. Sci.* **254** 5660
[30] Tang X G, Chan H L W and Chan A L 2004 *Thin Solid Films* **460** 227
[31] Cheng W X, Ding A L, He X Y, Zheng X S and Qiu P S 2006 *J. Electroceram.* **16** 523
[32] Xu J B, Zhai J W and Yao X 2007 *Ferroelectrics* **357** 166
[33] Anicete-Santos M *et al* 2005 *Chem. Phys.* **316** 260
[34] Cavalcante L S, Gurgel M F C, Paris E C, Simões A Z, Joya M R, Varela J A, Pizani P S and Longo E 2007 *Acta Mater.* **55** 6416
[35] Cavalcante L S, Gurgel M F C, Simões A Z, Longo E, Varela J A, Joya M R and Pizani P S 2007 *Appl. Phys. Lett.* **90** 011901
[36] Cavalcante L S, Anicete-Santos M, Sczancoski J C, Simões L G P, Santos M R M C, Varela J A, Pizani P S and Longo E 2008 *J. Phys. Chem. Solids* **69** 1782
[37] Joint Committee on Powder Diffraction Standards 2001 Diffraction Data File, no 36-0019, International Centre for Diffraction Data (ICDD, formerly JCPDS), Newtown Square, PA
[38] Holland T J B and Redfern S A T 1997 *Min. Mag.* **61** 65
[39] Maiti T, Alberta E, Guo R and Bhalla A S 2006 *Mater. Lett.* **60** 3861
[40] Maiti T, Guo R and Bhalla A S 2006 *J. Appl. Phys.* **100** 114109
[41] Moreira M L, Mambrini G P, Volanti D P, Leite E R, Orlandi M O, Pizani P S, Mastelaro V R, Paiva-Santos C O, Longo E and Varela J A 2008 *Chem. Mater.* **20** 5381
[42] Cavalcante L S, Sczancoski J C, Espinosa J W M, Mastelaro V R, Michalowicz A, Pizani P S, De Vicente F S, Li M S, Varela J A and Longo E 2009 *J. Alloys Compounds* **471** 253
[43] Domenico M D Jr, Wemple S H, Porto S P S and Buman P R 1968 *Phys. Rev.* **174** 522
[44] Chaves A, Katiyar R S and Porto S P S 1974 *Phys. Rev.* B **10** 3522
[45] Kreisel J, Bouvier P, Maglione M, Dkhil B and Simon A 2004 *Phys. Rev.* B **69** 092104
[46] Dobal P S, Dixit A, Katiyar R S, Yu Z, Guo R and Bhalla A S 2001 *J. Appl. Phys.* **89** 8085
[47] Begg B D, Finnie K S and Vance E R 1996 *J. Am. Ceram. Soc.* **79** 2666
[48] Dixit A, Majumder S B, Dobal P S, Katiyar R S and Bhalla A S 2004 *Thin Solid Films* **447** 284
[49] Karan N K, Katiyar R S, Maiti T, Guo R and Bhalla A S 2008 *J. Raman Spectrosc.* **40** 370
[50] Kakihana M 1960 *J. Sol–Gel Sci. Technol.* **6** 7
[51] Rahaman M N 2008 *Sintering of Ceramics* (Boca Raton, FL: CRC Press) (Taylor and Francis Group) pp 55–106
[52] Kang S J L 2005 *Sintering-Densification, Grain Growth and Microstructure* (Amsterdam: Elsevier) pp 39–91
[53] Ramasubramaniam A and Shenoy V B 2005 *Acta Mater.* **53** 2943
[54] Reddy S B, Rao K P and Rao M S R 2009 *J. Alloys Compounds* **481** 692
[55] Moreira M L, Gurgel M F C, Mambrini G P, Leite E R, Pizani P S, Varela J A and Longo E 2008 *J. Phys. Chem.* A **112** 8938
[56] Wang L M and Richert R 2005 *J. Phys. Chem.* B **109** 11091
[57] De Wilde P and Brebbia C A 2006 *High Performance Structures and Materials III* ed C A Brebbia (Southampton, UK: Wessex Institute of Technology) pp 252–26 (section 4) http://library.witpress.com/pages/list_Papers.asp?q_bid=341
[58] Tang X G, Wang J, Wang X X and Chan H L W 2004 *Solid State Commun.* **131** 163
[59] Shrout T R, Cross L E, Moses P, McKinstry H A and Neurgaonkar R 1980 A phenomenological theory for predicting the temperature dependence of elastic, dielectric and piezoelectric properties in simple proper ferroelectric crystals *Ultrasonics Symp.* pp 414–9
[60] Reddy S B, Rao K P and Rao M S R 2007 *Appl. Phys.* A **89** 1011
[61] Dixit A, Majumder S B, Katiyar R S and Bhalla A S 2003 *Appl. Phys. Lett.* **82** 2679
[62] Dixit A, Majumder S B and Katiyar R S 2007 *Frontiers of Ferroelectricity* pp 87–96

[63] Maiti T, Guo R and Bhalla A S 2007 *Appl. Phys. Lett.* **90** 182901
[64] Tang X G, Wang X X, Chew K-H and Chan H L W 2005 *Solid State Commun.* **136** 89
[65] Majlis N 2003 *The Quantum Theory of Magnetism* (Singapore: World Scientific) p 35
[66] Mattis D C 2006 *The Theory of Magnetism Made Simple: An Introduction to Physical Concepts and to Some Useful Mathematical Methods* (Singapore: World Scientific) pp 25–30
[67] Badapanda T, Rout S K, Panigrahi S and Sinha T P 2008 *Bull. Mater. Sci.* **31** 897
[68] Tang X G, Liu Q X, Wang J and Chan H L W 2009 *Appl. Phys.* A **96** 945
[69] Guo Y, Kakimoto K and Ohsato H 2004 *J. Phys. Chem. Solids* **65** 1831
[70] Rout S K, Badapanda T, Sinha E, Panigrahi S, Barhai P K and Sinha T P 2008 *Appl. Phys.* A **91** 101
[71] Wood D L and Tauc J 1972 *Phys. Rev.* B **5** 3144
[72] Cavalcante L S, Sczancoski J C, De Vicente F S, Frabbro M T, Siu Li M, Varela J A and Longo E 2009 *J. Sol–Gel Sci. Technol.* **49** 35
[73] Longo V M *et al* 2008 *Acta Mater.* **56** 2191